

Cosmic Ray Driven Outflows in an Ultraluminous Galaxy

Akimi Fujita,^{1*} and Mordecai-Mark Mac Low^{2†}

¹*Faculty of Engineering, Shinshu University, Nagano, Nagano, Japan*

²*Department of Astrophysics, American Museum of Natural History, New York, New York, U.S.A.*

Accepted 2018 Marh 17

ABSTRACT

In models of galaxy formation, feedback driven both by supernova (SN) and active galactic nucleus (AGN) is not efficient enough to quench star formation in massive galaxies. Models of smaller galaxies have suggested that cosmic rays (CRs) play a major role in expelling material from the star forming regions by diffusing SN energy to the lower density outskirts. We therefore run gas dynamical simulations of galactic outflows from a galaxy contained in a halo with $5 \times 10^{12} M_{\odot}$ that resembles a local ultraluminous galaxy, including both SN thermal energy and a treatment of CRs using the same diffusion approximation as [Salem & Bryan \(2014\)](#). We find that CR pressure drives a low-density bubble beyond the edge of the shell swept up by thermal pressure, but the main bubble driven by SN thermal pressure overtakes it later, which creates a large-scale biconical outflow. CRs diffusing into the disk are unable to entrain its gas in the outflows, yielding a mass-loading rate of only $\sim 0.1\%$ with varied CR diffusion coefficients. We find no significant difference in mass-loading rates in SN driven outflows with or without CR pressure. Our simulations strongly suggest that it is hard to drive a heavily mass-loaded outflow with CRs from a massive halo potential, although more distributed star formation could lead to a different result.

Key words: cosmic rays – galaxies: evolution – galaxies: haloes – galaxies:sby kinematics and dynamics

1 INTRODUCTION

In the theory of galaxy formation, feedback in the form of galactic outflows plays an important role in regulating star formation (SF), and thus the structure and evolution of galaxies. Outflows not only heat and ionize gas but can also drive gas and metal from SF regions to galactic haloes and beyond. Recent cosmological hydrodynamic simulations have highlighted the importance of suppressing SF with stellar feedback in galaxies towards the low mass end of the distribution and with active galactic nucleus (AGN) feedback in galaxies towards the high mass end to reproduce the observed, global properties of galaxies (e.g. [Vogelsberger et al. 2013](#); [Marinacci et al. 2014](#)). At the same time, these simulations showed discrepancies that require further investigation, one of which is overproduction of stars at the present epoch in galaxies with halo masses $M_h \gtrsim 10^{12} M_{\odot}$, even with a very energetic form of AGN feedback compared to previous studies ([Vogelsberger et al. 2014](#)). This mass, $\sim 10^{12} M_{\odot}$, seems to be the transition mass at which the main process regulating SF is stellar or supernova (SN) feedback below

and AGN feedback above. Cosmic rays (CRs) are suggested to be one of the major players in feedback. However, models of SN feedback in massive galaxies larger than the Milky Way have only included thermal pressure to date, not cosmic ray pressure (e.g. [Fujita et al. 2009](#); [Melioli & de Gouveia Dal Pino 2015](#)).

CRs can accelerate gas away from the dense ISM without radiatively losing energy, unlike thermal superbubbles ([Breitschwerdt et al. 1991](#)), and they lose less energy to adiabatic expansion than thermal gas. Recent three-dimensional (3D) hydrodynamic (HD) and magnetohydrodynamic (MHD) simulations have demonstrated that CR driven winds can smoothly accelerate colder, diffuse gas out of galactic disks and efficiently regulate SF in dwarf and Milky Way-like galaxies. ([Uhlir et al. 2012](#), [Hanasz et al. 2013](#), [Booth et al. 2013](#), [Salem & Bryan 2014](#); [Simpson et al. 2016](#), [Girichidis et al. 2016](#), [Martizzi et al. 2016](#), [Pakmor et al. 2016](#), [Ruszkowski et al. 2017](#)).

These works approximate CR transport with a variety of assumptions: 1) streaming at the local sound speed (HD: [Uhlir et al. 2012](#); [Wiener et al. 2017](#)); 2) self-confinement (MHD: [Ruszkowski et al. 2017](#)); 3) isotropic diffusion (HD: [Booth et al. 2013](#)), [Salem & Bryan 2014](#); or 4) anisotropic diffusion with fixed diffusion coefficients (MHD:

* E-mail: fujitaa@shinshu-u.ac.jp

† Email: mordecai@amnh.org

Hanasz et al. 2013; Girichidis et al. 2016), Pakmor et al. 2016; Ruszkowski et al. 2017. Wiener et al. (2017) in their study comparing streaming to diffusion point out that the dynamical effects of diffusion are overestimated by an order of magnitude when wave excitation and the transfer of energy from CRs to thermal gas by streaming are ignored in dwarf-sized galaxies, while Ruszkowski et al. (2017) demonstrate that the dynamical effects of streaming and diffusion are comparable if wave growth due to the streaming instability is inhibited by some damping process, such as turbulent damping, even in a Milky Way-sized galaxy.

The effects of CR pressure have not been studied in galaxies more massive than the Milky Way. We therefore run simulations of galactic outflows, including both SN thermal energy and cosmic rays, with varying isotropic coefficient of diffusion, in a massive galaxy that resembles a local ultraluminous galaxy some ~ 5 times than the Milky Way. Our galaxy and galactic outflow models are based on Fujita et al. (2009) with a halo mass $5 \times 10^{12} M_{\odot}$ and a mechanical luminosity $L_{mech} = 10^{43} \text{ erg s}^{-1}$ provided by supernova explosions and associated stellar outflows, and treated as a continuous energy input (Mac Low & McCray 1988). Our previous study showed that SN thermal feedback alone is not effective in driving a heavily mass-loaded outflow from its deep potential. Therefore, we compute the mass-loading rates of CR-driven outflows in the same galaxy with the same SF and superbubble recipe by including a diffusive CR fluid, as described in Salem & Bryan (2014). We assume that AGN feedback still remains quiescent in the galaxy.

In this paper, we describe our numerical methods as well as our disk and outflow models in Section 2 and the mass-loading rates, as well as resolution studies in Section 3, followed by discussion in Section 4 and conclusion in Section 5.

2 NUMERICS

2.1 Algorithm

The simulations were performed using the adaptive mesh refinement hydrodynamics code ENZO (e.g. Bryan et al. 2014) with a two-fluid model for CRs (Drury & Falle 1986) implemented and tested by Salem & Bryan (2014). In this model, CRs are treated as a relativistic gas with $\gamma_{CR} = 4/3$ that is coupled to the thermal plasma with $\gamma_{th} = 5/3$ except for a diffusion term. Bulk motions of the thermal gas transport the CRs, and they in turn diffuse and exert pressure on the thermal gas.

This model assumes that CRs diffuse isotropically by scattering off inhomogeneities in the tangled magnetic fields near the disk midplane, with a fixed CR diffusion coefficient κ_{CR} . Recent MHD simulations show that outflows develop later with anisotropic diffusion, but only in cases with magnetic fields dominated by azimuthal components (Pakmor et al. 2016), and that anisotropic diffusivities act similar to isotropic diffusivities with $\kappa_{CR} \sim \kappa_{||}/3$ where $\kappa_{||}$ is a fixed CR diffusion coefficient parallel to the magnetic fields (Ruszkowski et al. 2017). In both studies, the global mass-loading rates with anisotropic diffusion are comparable to those with isotropic diffusion.

We apply a ceiling to the effective sound speed of

$c_{s,max} = 2.05 \times 10^4 \text{ km s}^{-1}$ in low-density, CR-dominated cavities by raising the density within them in the highest resolution run (QC: see Table 1). This is necessary to prevent our computation from slowing down significantly, but only a very small portion of the gas feels this effect, causing no significant change in the dynamics (Salem & Bryan 2014).

2.2 Cosmic Ray Parameters

We choose values of the diffusion coefficient $\kappa_{CR} = 3 \times 10^{27} \text{ cm}^2 \text{ s}^{-1}$, which yielded the highest mass-loading rate of ~ 1.0 in Salem & Bryan (2014), and an order of magnitude higher and lower. Salem & Bryan (2014) found that low diffusion rates prevent CRs from diffusing out of the densest regions quickly enough to create the pressure gradient in the upper atmosphere of the disk required to accelerate more mass, while high diffusion rates release the cosmic rays before they can couple to the gas effectively. Our central value corresponds to $\kappa_{||} = 1 \times 10^{28} \text{ cm}^2 \text{ s}^{-1}$ according to Ruszkowski et al. (2017).

SNe are thought to convert a fraction $f_{CR} = 0.1$ to $\gtrsim 0.5$ of their kinetic energy into CRs by diffusive shock acceleration (see review by Helder et al. 2012). We choose to use $f_{CR} = 0.3$ to be consistent with Salem & Bryan (2014), noting that this is larger than the value of $f_{CR} = 0.1$ used in most studies in this field.

For runs including CRs, an initial CR energy density η_{CR} is assigned with a value proportional to the initial gas density in each cell $\eta_{CR} = \alpha_{CR} \times \rho$ to mimic the CR energy density distribution of the solar neighborhood at the midplane of $\eta_{CR} \sim 3 \times 10^{-12} \text{ erg cm}^{-3}$ (Salem & Bryan 2014), where $\alpha_{CR} = 10^7$. The CR energy density in starburst galaxies is likely much higher (Acciari et al. 2009; Papadopoulos 2010), but the initial distribution has a negligible effect on the results, as CRs generated by SNe quickly diffuse and dominate the CR dynamics.

2.3 Disk Model

We use disk and star formation models for an ultraluminous infrared galaxy (ULIRG) from Fujita et al. (2009). This model has a disk gas mass, $M_g = 10^{10} M_{\odot}$, a surface density $\Sigma_0 = 10^4 M_{\odot} \text{ pc}^{-2}$, and an exponential scale radius $R_d = 0.7 \text{ kpc}$. The gravitational potential includes a disk potential based on the thin disk approximation (Toomre 1963), and a Navarro et al. (1997) halo potential from a halo with mass $M_h = 5 \times 10^{12} M_{\odot}$, virial radius $R_v = 326 \text{ kpc}$, and halo concentration factor $c = 5$. We assume the gas is supported by turbulence with a high velocity dispersion $\sigma = 55 \text{ km s}^{-1}$, comparable to that observed in the molecular gas in Arp220 (Scoville et al. 1997).

Only half the disk above its midplane is simulated, in an initial grid whose size varies with the finest resolution employed. This was necessary to save computation time, because the computation of CR diffusion requires time steps that are proportional to the square of the finest resolution size

$$\Delta t_{CR} < \frac{1}{6} \frac{\Delta x^2}{\kappa_{CR}}. \quad (1)$$

2.4 Cooling

The radiative cooling curve of Sarazin & White (1987), with a temperature floor $T_{min} = 10^4$ K is used, based on the assumption that the gas is kept photoionized by UV radiation from massive stars. This temperature floor has a negligible effect on the dynamics because cooling in the swept-up shells is limited by numerical resolution, rather than by radiative cooling (Fujita et al. 2009).

We note that the CR cooling losses due to Coulomb and catastrophic interactions that we neglect could be significant in our dense ULIRG disk: for example, the cooling time due to catastrophic losses alone is rather short, only a few years at $\rho \sim 2 \times 10^{-20}$ g cm $^{-3}$ (Jubelgas et al. 2008). We do not model the CR spectrum that would be required for the realistic cooling calculation. The CR cooling time, both Coulomb and catastrophic, is inversely proportional to the gas density, so CR cooling losses become negligible once the CRs diffuse out of the dense disk to its low-density outskirts and the halo beyond.

2.5 Starburst

We assume a single starburst that occurs at the center of the disk. All the kinetic energy of the starburst SNe is released in a central wind of constant mechanical luminosity, $L_{mech} = 10^{43}$ erg s $^{-1}$. This approximation can be made because the discrete energy inputs from SNe generate blast-waves that become subsonic in the hot interior of the bubble first produced by stellar winds (Mac Low & McCray 1988; Fujita et al. 2009). This assumption means that a single superbubble forms, evolving to produce a bipolar outflow of gas. We chose $L_{mech} = 10^{43}$ erg s $^{-1}$ as it corresponds to the mechanical luminosity expected during the first 2 Myr after the onset of an instantaneous starburst with $M_* = 10^9 M_\odot$ or of continuous star formation with $100 M_\odot \text{ yr}^{-1}$ at ~ 2 Myr or $500 M_\odot \text{ yr}^{-1}$ at ~ 4 Myr (Leitherer et al. 1999). Energy input is continued for the entire duration of our simulations in this study, as our simulation time is much less than the lifetime of the smallest B star to go supernova. Bubbles in our highly stratified, ULIRG disk blow out within 1 Myr. We note that it is an oversimplification to assume a single starburst site at the disk center, as some ULIRG winds appear to require starburst regions extended to > 1 kpc (Martin 2006). Modeling multiple star forming regions remains as future work.

To drive a constant luminosity wind, we add mass and energy to a source region (Mac Low & Ferrara 1999) with a radius of five zones for the runs with a finest resolution of 6.4 pc and with a radius of 5 pc for the runs with finest resolutions of 0.8 pc and 0.2 pc. The fiducial mass input rate is $\dot{M}_{in} = 4.7 M_\odot \text{ yr}^{-1}$ to be consistent with Fujita et al. (2009). However, as we show later, the mass in outflows is dominated by this injected mass, \dot{M}_{in} , so we also ran the simulations with a mass input rate, $\dot{M}_{in} = 0.47 M_\odot \text{ yr}^{-1}$, an order of magnitude lower than the fiducial value. The corresponding temperatures of the hot, shocked, bubble interior gas are $T_{in} = 1.4 \times 10^8$ and 1.4×10^9 K respectively. Radiative cooling is turned off in the hot bubble interior with a steepened tracer field c (Yabe & Xiao 1993). The field

$$f(c) = \tan[0.99\pi(c - 0.5)]. \quad (2)$$

Table 1. Numerical models

Model	Physics ^a	Δx_{min} (pc)	base	AMR ^b	κ_{CR}^c	\dot{M}_{in}^d
F09	T	0.2	64 ³	6	–	4.7
Q	T/C	0.8	64 ³	4	10	4.7
W	T/C	3.2	16 ² × 32	3	10	4.7
X	T/C	6.4/12.8	16 ³	4	10	4.7
Z	T/C	6.4/12.8	16 ³	4	10	0.47
ZI	C	6.4/12.8	16 ³	4	1	0.47

^aSN contribution: T = Thermal pressure; C = Cosmic rays

^bNumber of adaptive mesh refinement levels

^cIn units of 3×10^{26} cm 2 s $^{-1}$

^dMass input rates in units of $M_\odot \text{ yr}^{-1}$

is advected, accumulating diffusion errors that smooth out sharp interfaces, but the inverse field $c(f)$ is factored into the cooling function, maintaining sharp transition interfaces (Mac Low & Ferrara 1999; Fujita et al. 2004). This prevents mass numerically diffused from the cold, dense shell into the rarefied, hot interior from spuriously cooling the interior, as the cooling time of the interior is much longer than the dynamical time of our bubble (Mac Low & McCray 1988).

2.6 Models

Table 1 lists the diffusion coefficients and numerical resolutions of our models. For comparison, Salem & Bryan (2014) used a resolution of $\Delta x_{min} = 61$ pc. Because of the diffusive time step condition (Eq. 1), the computation becomes quadratically more expensive with finer resolution. To reproduce Fujita et al. (2009) would require $\Delta x_{min} = 0.2$ pc in a $(0.2 \text{ kpc})^3$ box, which is impractical to do with CRs using available resources. We had to reduce the resolution to 6.4 pc in the disk and 12.8 pc outside the disk in a $(3.3 \text{ kpc})^3$ box, in order to study the effects of CR pressure in the halo out to a few kiloparsecs above the disk.

We compare the mass-loading rates of outflows driven only by SN thermal pressure (T) and driven both by SN thermal pressure and CR pressure (C) in models Q, W, and X with varying resolutions. In the highest resolution model F09, which reproduces the 2D model of Fujita et al. (2009) in 3D, we run a simulation of an outflow driven by SN thermal pressure alone. We also run the lowest resolution model with a low mass injection rate, Z, and we test the effects of varying diffusion coefficients using the lowest resolution models, ZI and ZC.

3 RESULTS

Figure 1 shows our 3D version F09 of the fiducial 2D model by Fujita et al. (2009) of a galactic outflow driven by SN thermal pressure alone with $\Delta x_{min} = 0.2$ pc using 6 levels of refinement. The kinematic behaviour of the outflow agrees between the previous 2D simulation and our 3D version. The shocked swept-up shells of ambient gas fragment by Rayleigh-Taylor (RT) instability, showing the usual spike and bubble morphology. Most fragments travel at a few hundred kilometers per second, while a small fraction of them exceed the escape velocity $v_{esc} = 800 \text{ km s}^{-1}$ at $0.01 R_v$.

We do find that the 3D computation resolves the growth

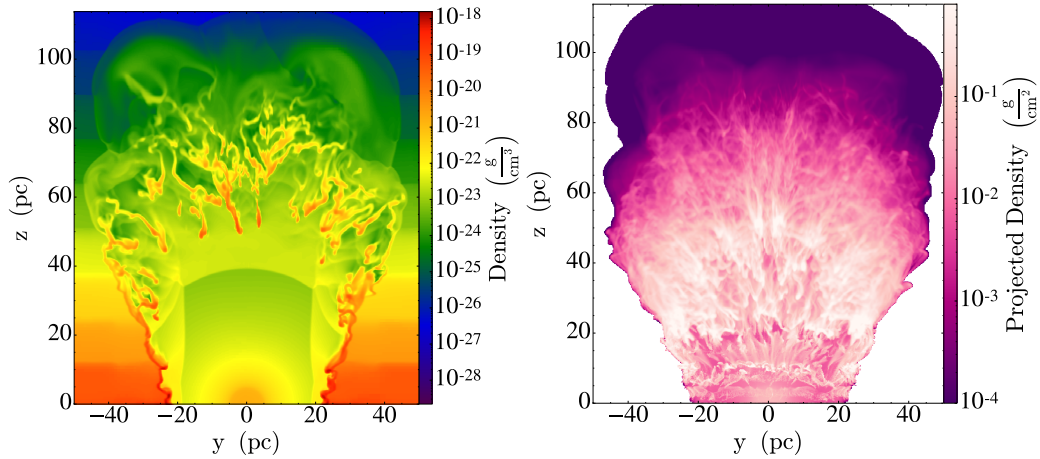


Figure 1. A density slice at the center (*left*); and a projected density distribution (*right*) of a thermal pressure driven outflow blowing out of the disk at $t \sim 0.16$ Myr in our highest resolution run F09, with $\Delta x_{min} = 0.2$ pc. The fine resolution in 3D resolves the fragmentation of the swept-up shells into spikes by Rayleigh-Taylor instability. We confirm that our 3D result is consistent with our previous 2D result (Fujita et al. 2009) in the kinematic behaviour of the hot interior and the cooler shells. Only gas moving at $v_z > 0$ is used for the projection, to exclude quiescent background gas in the disk and halo. Note that the color scales used are the same as in Figure 3 and Figure 6 below.

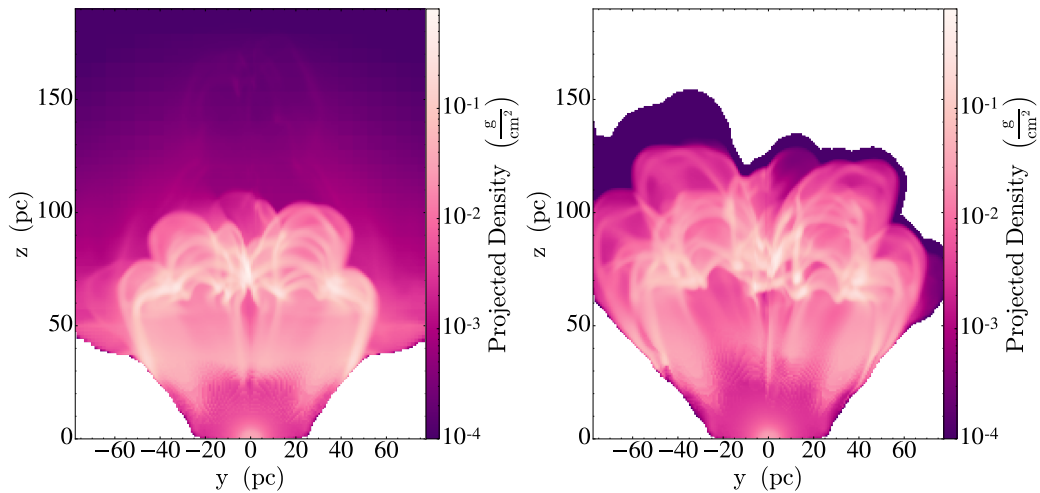


Figure 2. Projected density distributions of a CR pressure driven outflow (QC; *left*) and a thermal pressure driven outflow (QT; *right*) blowing out of the disk at $t \sim 0.27$ Myr in our highest resolution run with $\Delta x_{min} = 0.8$ pc. At this time, the thermally driven shock has grown faster, but CRs diffusing out from the CR driven bubble have already accelerated the halo gas above. Again only the gas moving at $v_z > 0$ is used for the projected density distribution.

of RT spikes, while in 2D, the assumption of azimuthal symmetry limited RT instabilities to grow as rings, decreasing the extent of fragmentation. Figure 1 shows the hot, low-density interior gas streaming through the spikes, ablating their outer layers by Kelvin-Helmholtz instability.

Figure 2 compares projected density distributions of a superbubble driven by SN thermal pressure alone (QT) and a superbubble driven by both SN thermal and CR pressure (QC), blowing out of the disk at $t = 0.27$ Myr in runs with $\Delta x_{min} = 0.8$ pc. Only gas rising vertically out of the disk at $v_z > 0$ km s⁻¹ is projected in the figure to exclude the quiescent disk and halo gas. The classic thermal pressure driven superbubble (QT) is larger, with the shell fragmenting, and letting the hot gas escape, compared to the CR driven superbubble with CRs quickly diffusing into the disk beyond the swept-up shells and out into the halo.

The resulting CR pressure gradient accelerates the low-density halo gas to $v > 500$ km s⁻¹, and in particular, drives a low-density bubble beyond the outer edge of the swept-up shells that travels at $v > 1000$ km s⁻¹, as shown in Figure 3. This bubble initially expands faster into the halo than the thermal pressure driven shock, but it only carries $\sim 10\%$ of the total mass traveling at $v > 1000$ km s⁻¹ on the grid in model QC. The total mass moving upwards with vertical velocity $v_z > 10$ km s⁻¹ and speed exceeding the turbulent sound speed $|\mathbf{v}| > c_s = 55$ km s⁻¹ is $1.5 \times 10^6 M_\odot$ in the thermal-pressure driven case and $1.8 \times 10^6 M_\odot$ in the CR driven case, only a modest increase. For the mass-loading calculation, we exclude mass moving at $v_z \leq 10$ km s⁻¹ in order to only include gas accelerated by bubbles. Note that the gas moving with $v_z = 10$ km s⁻¹ will travel only ~ 5 kpc upward in 500 Myr if it maintains its speed.

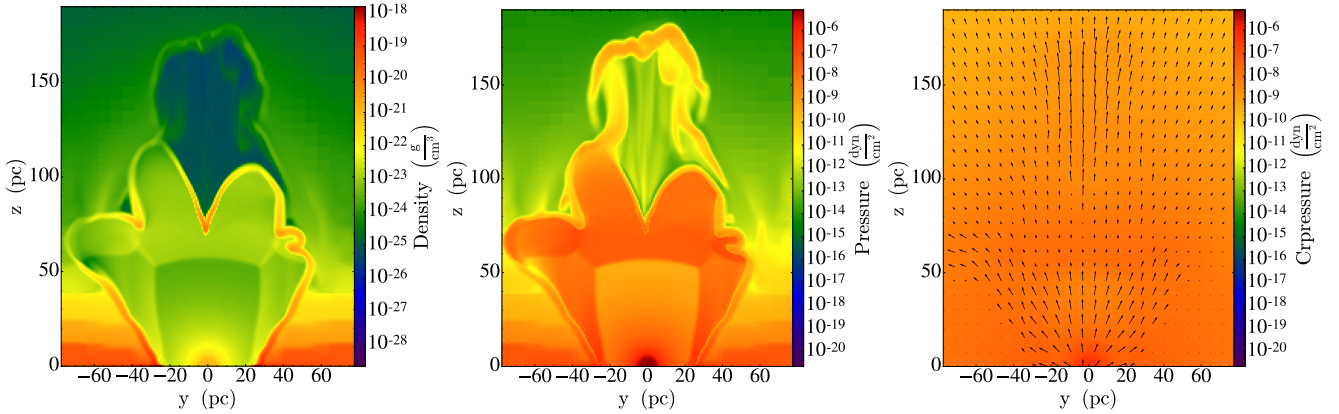


Figure 3. Slices of density (*left*), pressure (*middle*), and CR pressure overlaid with velocity (*right*) in the plane in a CR pressure driven outflow at $t \sim 0.27$ Myr in model QC. The CR pressure gradient across the outer edges of the swept-up shell drives a low density bubble that expands into the halo at $v > 1000 \text{ km s}^{-1}$ ahead of the thermal pressure driven superbubble. The maximum velocity shown is $v_{max} = 3700 \text{ km s}^{-1}$. Note that the color scales used are the same as in Figure 1 and Figure 6 below.

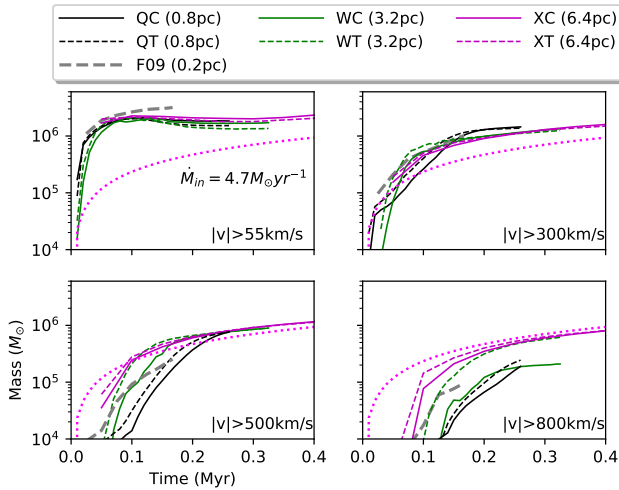


Figure 4. Total mass with (*solid*) and without (*dashed*) CR pressure in outflows moving upward ($v_z > 10 \text{ km s}^{-1}$) with speeds $|v| > 55 \text{ km s}^{-1}$, $|v| > 300 \text{ km s}^{-1}$, $|v| > 500 \text{ km s}^{-1}$, and $|v| > 800 \text{ km s}^{-1}$ in our models with a mass injection rate $\dot{M}_{in} = 4.7 \text{ M}_{\odot} \text{ yr}^{-1}$ (cumulative input mass shown in *magenta dotted*) at varying resolutions given in the legend. We only have results up to $t \sim 0.15$ Myr for the highest resolution run (*dashed gray*) due to limited computational resources, but the total mass moving at $|v| > 55 \text{ km s}^{-1}$ seems to have already reached a plateau. Only a small fraction of mass is moving out into the halo. The total mass in outflows with varying resolutions converges well after $\sim 0.2\text{--}0.3$ Myr, but it is dominated by the SN ejecta mass \dot{M}_{in} that generates the outflows, rather than by entrained gas.

In order to study the effects of CR pressure accelerating mass, we ran the same simulations on larger grids covering several kiloparsecs in the halo, by reducing the resolution (Table 1). Figure 4 shows a resolution study of the total mass in outflows modeled with varying resolutions, with and without CR pressure. The mass injection rate for these runs is $\dot{M}_{in} = 4.7 \text{ M}_{\odot} \text{ yr}^{-1}$. The peaks of mass entrainment tend to occur later in the higher-resolution runs because blowout occurs later due to the smaller sizes of their source regions

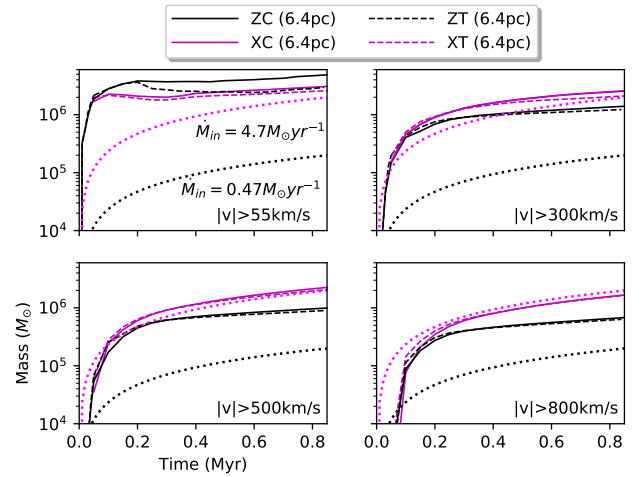


Figure 5. Total mass with (*solid*) and without (*dashed*) CR pressure in outflows moving upward ($v_z > 10 \text{ km s}^{-1}$) with speeds $|v| > 55 \text{ km s}^{-1}$, $|v| > 300 \text{ km s}^{-1}$, $|v| > 500 \text{ km s}^{-1}$, and $|v| > 800 \text{ km s}^{-1}$ in our lowest resolution models ($\Delta x = 6.4/12.8 \text{ pc}$) with mass injection rates, $\dot{M}_{in} = 4.7 \text{ M}_{\odot} \text{ yr}^{-1}$ (cumulative mass injected in *magenta dotted*) and $\dot{M}_{in} = 0.47 \text{ M}_{\odot} \text{ yr}^{-1}$ (*black dotted*). The amount of mass carried in the outflows is approximately the same independent of the mass input that we use to generate the outflows.

(which have constant size in zones), but after the peaks, the total masses converge within a factor of a few. All models seem to converge well after $\sim 0.2\text{--}0.3$ Myr, as the outflow structures are fully developed by this time. However, by the same time, the total mass of outflow gas is nearly equal to the mass we inject to generate the outflow (*dotted* in Figure 4).

In order to differentiate ambient gas from injected mass in the outflows, we run simulations with a mass injection rate an order of magnitude smaller than the fiducial value, $\dot{M}_{in} = 0.47 \text{ M}_{\odot} \text{ yr}^{-1}$, using the lowest resolution (Z) since the resulting extremely hot interior gas lowers the timestep substantially. Figure 5 shows $\sim 10^6 \text{ M}_{\odot}$ of disk gas is accelerated in the outflow in Z runs, and total outflow masses are

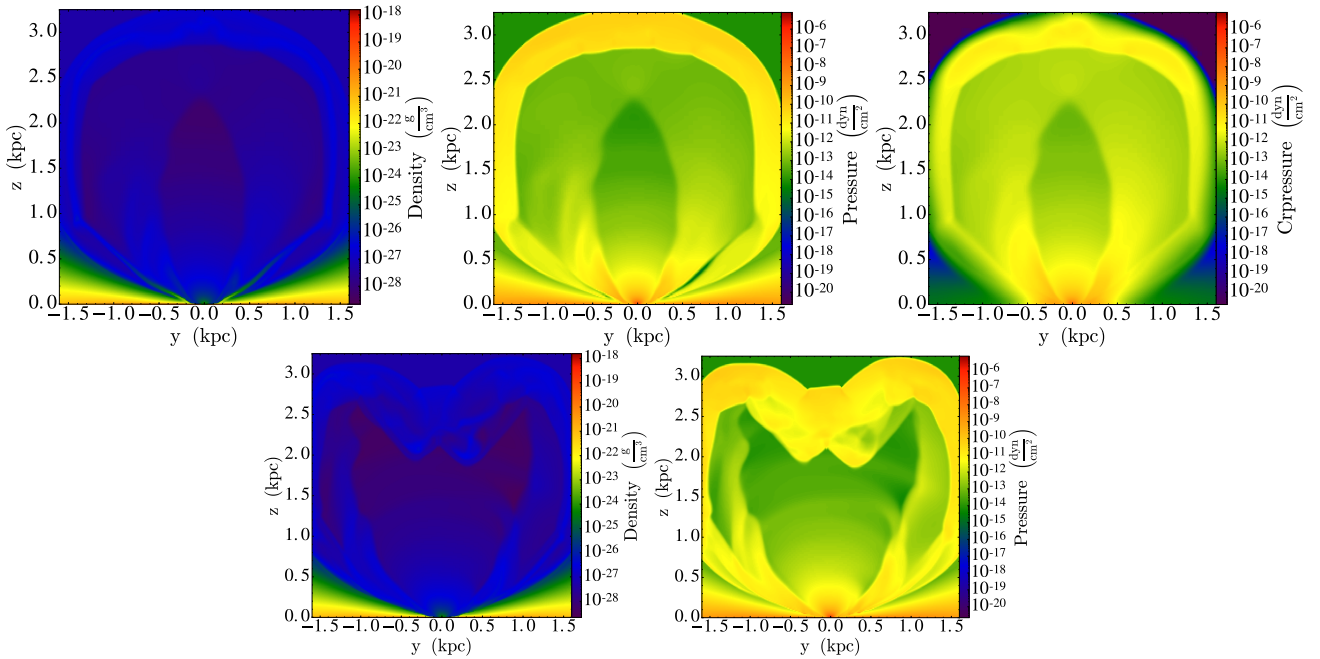


Figure 6. Slices of density (left), pressure (middle), and CR energy and gas velocity (right) distributions in a CR pressure driven outflow (ZC: top), and slices of density (left) and pressure (right) distributions in a thermal pressure driven outflow (ZT: bottom) in our lowest-resolution run ($\Delta x_{min} = 6.4$ pc in the disk and 12.8 pc outside) that covers several kiloparsecs in the halo at $t = 1.2$ Myr. The mass injection rate is $\dot{M}_{in} = 0.47 M_{\odot} \text{ yr}^{-1}$. By this time, the thermal pressure driven shock has overtaken the low-density bubble created by CR pressure earlier in Figure 3, and both CR pressure and thermal pressure driven outflows are behaving similarly. Note that the color scales used are the same as in Figure 1 and Figure 3.

the same within a factor of two, whether the mass injection rate is 4.7 or $0.47 M_{\odot} \text{ yr}^{-1}$, with or without CR pressure. The small difference is due to the temperature difference of the bubble interiors: there is less cooling of numerically diffused gas from the swept-up shells in a hotter, lighter bubble than a cooler, denser bubble.

The mass entrained is plotted in multiple velocity ranges because previous studies suggested that the gas accelerated by CR pressure is more diffuse, and moves at much lower velocity than the gas accelerated by SN thermal pressure, which moves at higher velocity due to its higher sound speed (Salem & Bryan 2014; Simpson et al. 2016; Girichidis et al. 2016; Pakmor et al. 2016). In our simulations, there is no noticeable difference in mass-loading rates with and without CR pressure, so this trend is absent.

The convergence we find after the peaks in outflow masses allows us to use the lowest resolution runs to study the effects of CR pressure at later times when the outflows spread out to a few kiloparsecs in the halo. Figure 6 shows outflows in our model disk with and without CR pressure at $t = 1.2$ Myr. Our disk is very thin due to our massive disk potential with a disk gas mass $M_g = 10^{10} M_{\odot}$ and a surface density $\Sigma_0 = 10^4 M_{\odot} \text{ pc}^{-2}$. It flares out to a few hundred parsecs at the exponential scale radius $R_d = 0.7 \text{ kpc}$ and reaches a thickness of $\sim 1 \text{ kpc}$ at $\sim 2R_d$.

In simulation ZC, we find that by $t \sim 0.4$ Myr, the thermal-pressure driven superbubble catches up with the low-density CR driven bubble above it, and eventually overtakes it, and pushes it to the side. CRs quickly diffuse through the disk and the upper atmosphere outside the shells swept-up by the superbubble, for example, to a radius of

$\gtrsim 0.5 \text{ kpc}$ by $t = 1.2$ Myr. (top right in Figure 6). However, most of the disk gas remains tightly bound in the galactic potential, not entrained in the outflow. As a result, both CR pressure and thermal pressure driven outflows behave quite similarly. CR pressure can accelerate $\sim 60\%$ more mass than thermal pressure alone at vertical velocity $v_z > 10 \text{ km s}^{-1}$, and $\sim 45\%$ at $v_z = 55 \text{ km s}^{-1}$. The total mass moving is only $3.1 \times 10^6 M_{\odot}$ and $2.7 \times 10^6 M_{\odot}$ respectively, even in the CR-driven outflow.

Figure 7 shows the density, CR pressure, and the ratio of CR pressure to the combined thermal and CR pressure defined as $\epsilon = P_{CR}/(P_{CR} + P_{TH})$ for model ZC at $t = 2.2$ Myr in the disk where most mass is. The outflow is dominated by CR pressure with $\epsilon > 0.5$, but both CR and thermal pressure keep pushing the disk gas to the side, pressing it to the midplane, instead of entraining it in the outflow. The compressed, high-density gas at the midplane is where most displaced mass is, dominated by thermal pressure.

We also ran a simulation ZI with a CR diffusion coefficient $\kappa_{CR} = 3 \times 10^{26} \text{ cm}^2 \text{ s}^{-1}$ an order of magnitude smaller than our fiducial value, to be compared to our model ZC. Salem & Bryan (2014) showed that mass-loading is more efficient with their smallest CR diffusion coefficient, $\kappa_{CR} = 3 \times 10^{27} \text{ cm}^2 \text{ s}^{-1}$, compared to values one or two orders of magnitude higher that they also tested, because CRs remain in higher-density regions longer to exert pressure on the gas. (We chose $\kappa_{CR} = 3 \times 10^{27} \text{ cm}^2 \text{ s}^{-1}$ as our fiducial value, based on their results.)

CRs indeed diffuse more slowly in model ZI than model ZC, so they remain in the central few hundred parsec region of the disk longer, instead of diffusing out into the cavi-

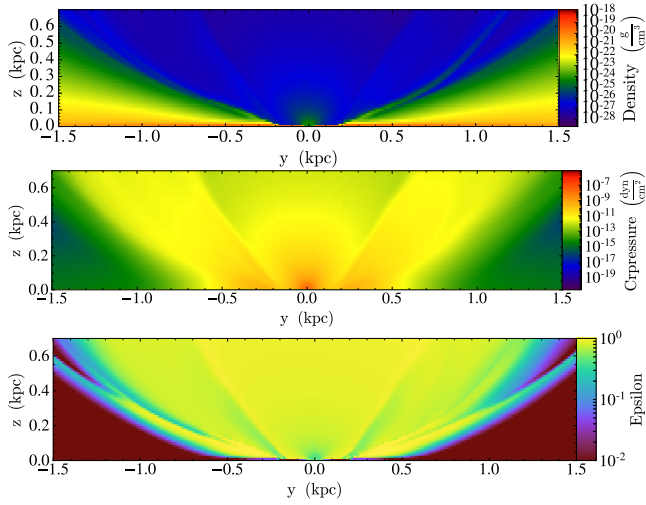


Figure 7. Slices of density (*top*), CR pressure (*middle*), and epsilon (*bottom*) distributions in the disk with a CR driven outflow with a diffusion coefficient $\kappa_{CR} = 3 \times 10^{27}$ (ZC) in our lowest-resolution runs ($\Delta x_{min} = 6.4$ pc in the disk and 12.8 pc outside) at $t = 2.2$ Myr. The mass injection rate is $\dot{M}_{in} = 0.47 M_{\odot} \text{ yr}^{-1}$. CRs diffuse out to the halo and into the disk, dominating the pressure in the outflow, but are unable to entrain the disk gas.

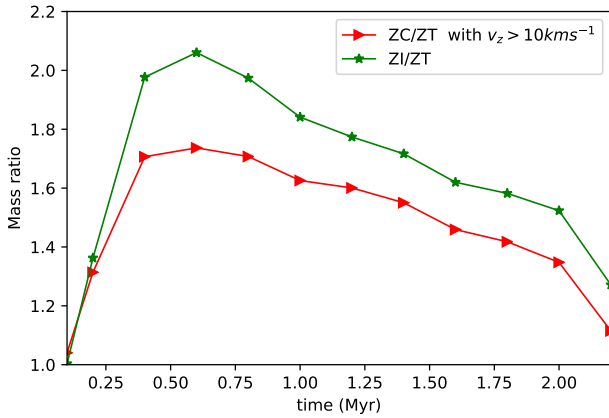


Figure 8. The ratio of total mass in CR-driven outflows to total mass in thermally-driven outflow, with CR diffusion coefficients $\kappa_{CR} = 3 \times 10^{27}$ (ZC; *red triangle*) and $3 \times 10^{26} \text{ cm}^2 \text{ s}^{-1}$ (ZI; *green star*). Outflow mass includes all mass moving upward with $v_{z,min} = 10 \text{ km s}^{-1}$. CR pressure initially loads about twice as much mass as thermal pressure alone at blowout, but does not seem to accelerate more mass afterwards.

ties created by the outflows. Nevertheless, the total mass moving in model ZI remains similar to that in model ZC, with $3.5 \times 10^6 M_{\odot}$ at $v_z > 10 \text{ km s}^{-1}$ and $3.0 \times 10^6 M_{\odot}$ at $v_z = 55 \text{ km s}^{-1}$ at $t = 1.2$ Myr.

Figure 8 shows that there is less than a factor of two difference in the total mass moving upward in outflows with or without CRs, with varied diffusion coefficients. All the extra mass in CR-driven outflows is accelerated by the time the main bubbles blow out at $t = 0.2\text{--}0.4$ Myr. The difference in loaded mass between CR-driven and thermal-pressure driven

outflows decreases as mass accelerated earlier by CRs moves off the computational grids. CRs no longer seem to entrain mass in the outflows.

We define the mass-loading ratio as the ratio of the amount of mass moving upward to the star formation rate. The total mass in the outflow is not likely to increase for $t > 2.2$ Myr (see Figure 7 and Figure 8), so we calculate the mass-loading ratios using the amount of accelerated mass at $t = 1.2$ Myr before a large part of it leaves the computational grid. If we assume an instantaneous starburst of $10^9 M_{\odot}$, the mass-loading ratio is only 0.003–0.004 while if we assume continuous star formation at a rate of $100\text{--}500 M_{\odot} \text{ yr}^{-1}$, we get mass-loading ratios of $\ll 0.006\text{--}0.03$.

We find that only slightly more gas is entrained from the disk and accelerated with CR pressure than with thermal pressure alone. With a single star formation site at the center of a disk, there is little substantive difference in SN driven outflow dynamics with or without CR pressure. This result holds despite our assignment of 30% of mechanical energy to CRs, choice of the assumption of isotropy in CR diffusion, and neglect of CR cooling.

In our simulations, the amount of mass that gains enough energy to reach the halo is determined at the time of blowout: this is what we expect for feedback by a classic thermal pressure driven wind based on previous numerical studies (Mac Low & Ferrara 1999; Fujita et al. 2009). Our simulations suggest that in a large, ultraluminous starburst galaxy with a single major SF site at the center, CRs do not seem to play any significant role in removing gas from its dense disk and massive halo potential.

4 MISSING PHYSICS

We neglected many pieces of physics for our study, including anisotropic diffusion and streaming of CRs, magnetic fields, CR spectrum spectral evolution and cooling, and realistic star formation distributions. We justify our choice to ignore the first five pieces of CR related physics in the list above by noting that our aim was to compute the maximum effect of CR pressure in our model galaxy with a single central SF site, within our limited computation time. Recent simulations with isotropic or anisotropic CR diffusion and CR streaming with or without MHD have shown that the assumption of isotropic diffusion leads to the highest mass-loading rate in a given numerical setting for a galaxy (e.g. Wiener et al. 2017; Ruszkowski et al. 2017).

On the other hand, the soft, ultrarelativistic, polytropic equation of state with $\gamma_{CR} = 4/3$ that we assume is likely to reduce the effects of CR pressure compared to the stiffer CR fluid expected from a larger spectral index for the CR energy distribution (Jubelgas et al. 2008). However, our simulations show that the overall outflow dynamics varies little whether it is driven only by thermal pressure or by both CR and thermal pressure, once the thermal pressure driven superbubble overtakes the low-density CR driven bubble as shown in Figure 6. In addition, our simulations show that the results do not depend significantly on the strength of CR diffusion.

We assumed a single SF site at the center of our disk to reproduce our previous results (Fujita et al. 2009) but clearly this is an oversimplification. We solved for the evo-

lution of a single, centrally concentrated starburst bubble based on superbubble dynamics in a single OB association: stellar winds create a hot, low-density cavity in the interstellar medium, and repeated SNe excavate a larger hole as they sweep the gas into a thin, dense shell (Tomisaka & Ikeuchi 1986; Mac Low & McCray 1988). A single energy source transfers energy to the surrounding rarefied interior gas more efficiently than multiple smaller clusters or single SNe spread over a large region in a disk (Fragile et al. 2004), because SN thermal energy dumped in high-density gas is vulnerable to radiative cooling. This means in our simulations, we are computing the maximum effects of SN thermal pressure on accelerating gas. However, a single superbubble sweeps the ISM but pushes most of it to the sides, as it blows out, so that only a small amount of swept-up gas is unbound from the disk. Although CRs that quickly diffuse isotropically through the disk and into the halo can further accelerate this small amount of swept-up material, our simulations show that they do not entrain mass from elsewhere in the upper atmosphere, as seen in models presented by, for example, Salem & Bryan (2014) and Girichidis et al. (2016). As a result, there is virtually no difference between mass-loading rates of outflows driven only by SN thermal pressure and of outflows driven both by SN thermal pressure and CR pressure.

Because our initial conditions do not include the effects of star formation feedback in forming a thick gas disk (the Lockman and Reynolds layers in our own galaxy, for example) our model does not have an extended moderate-density upper atmosphere to provide mass for CR acceleration as occurred in the earlier models.

The tunnel to vacuum provided by our single, central superbubble may also play a role in reducing the effect of CR acceleration on other parts of the disk. However, recent simulations of CR driven winds that find high mass-loading rates treat star formation over the entire disk wherever the gas density exceeds a certain threshold density (Uhlir et al. 2012; Hanasz et al. 2013; Booth et al. 2013; Salem & Bryan 2014; Simpson et al. 2016; Girichidis et al. 2016; Martizzi et al. 2016; Pakmor et al. 2016; Ruzsowski et al. 2017). CR pressure won't manage to unbind rotationally supported, orderly gas in a disk, but we suspect it might have a bigger impact on gas locally disturbed by superbubbles. We plan to address the dependence of mass-loading on star formation distribution in future work. Escaping CRs may also decelerate infalling gas in a halo, or even accelerate it outward, thus inhibiting it from feeding further star formation in a disk.

5 CONCLUSIONS

Our goal in this work was to answer the question of whether cosmic rays could enhance the ability of strong stellar feedback to drive galactic outflows in massive galaxies just below the mass where AGN feedback begins to dominate. To answer this question, we presented the results of 3D, hydrodynamic simulations of galactic outflows driven both by SN thermal pressure and CR pressure with isotropic CR diffusion in an ultraluminous galaxy with mass $5 \times 10^{12} M_{\odot}$. We modeled a single SF site at the center of the disk, and in this setting, we computed the maximum effect of CR pressure

on driving an outflow by neglecting several pieces of physics. CRs diffuse quickly through the disk and into the halo. They can drive a low-density bubble that expands beyond the shell swept up by the thermal pressure driven bubble. However, we find that the overall outflow dynamics are quite similar whether the outflow is driven by thermal pressure alone or by the combination of thermal and CR pressure, yielding a negligible difference between the mass-loading rates. Running simulations with varying CR diffusion coefficients did not change this result.

CRs appear to make little difference in this luminosity range, producing outflows with almost as little mass-loading as thermal driving alone. The path to vacuum opened up in the models by well-resolved thermal gas allows the CRs to escape easily, something that many previous models have not treated in detail.

Previous studies on SN feedback in galaxies have shown that dark matter is key to controlling whether a bubble blows out or blows away (e. g. Mac Low & Ferrara 1999), and likewise, dark matter may be key to the development of CR-driven outflows. However, we also speculate that simulations with multiple star forming regions distributed in space and time may change the result because CRs can entrain and accelerate extended, turbulent, moderate to low density upper atmosphere created by previous generations of star formation more efficiently than rotationally supported disk gas bound in the galactic potential.

ACKNOWLEDGEMENTS

M-MML was partly supported by NSF grant AST11-09395. We acknowledge use of the Fujitsu FX10 at Shinshu University, the Cray XC30 at the NAOJ, and resources from NSF XSEDE under grant TG-MCA99S024. Computations described in this work were performed using the publicly-available *Enzo* code (<http://enzo-project.org>), which is the product of a collaborative effort of many independent scientists from numerous institutions around the world. Their commitment to open science has helped make this work possible.

REFERENCES

- Acciari V. A., et al., 2009, *Nature*, 462, 770
 Booth C. M., Agertz O., Kravtsov A. V., Gnedin N. Y., 2013, *ApJ*, 777, L16
 Breitschwerdt D., McKenzie J. F., Volk H. J., 1991, *A&A*, 245, 79
 Bryan G. L., et al., 2014, *ApJS*, 211, 19
 Drury L. O., Falle S. A. E. G., 1986, *MNRAS*, 223, 353
 Fragile P. C., Murray S. D., Lin D. N. C., 2004, *ApJ*, 617, 1077
 Fujita A., Mac Low M.-M., Ferrara A., Meiksin A., 2004, *ApJ*, 613, 159
 Fujita A., Martin C. L., Mac Low M.-M., New K. C. B., Weaver R., 2009, *ApJ*, 698, 693 (F09)
 Girichidis P., et al., 2016, *ApJ*, 816, L19
 Hanasz M., Lesch H., Naab T., Gawryszczak A., Kowalik K., Woltanski D., 2013, *ApJ*, 777, L38
 Helder E. A., Vink J., Bykov A. M., Ohira Y., Raymond J. C., Terrier R., 2012, *Space Sci. Rev.*, 173, 369
 Jubelgas M., Springel V., Enßlin T., C. P., 2008, *A&A*, 481, 33
 Leitherer C., et al., 1999, *ApJS*, 123, 3

- Mac Low M.-M., Ferrara A., 1999, *ApJ*, 513, 142 (MF99)
- Mac Low M.-M., McCray R., 1988, *ApJ*, 324, 76
- Marinacci F., Pakmor R., Springel V., 2014, *MNRAS*, 437, 1750
- Martin C. L., 2006, *AJ*, 647, 222
- Martizzi D., Fielding D., Faucher-Giguere C.-A., Quataert E., 2016, *MNRAS*, 459, 2311
- Melioli C., de Gouveia Dal Pino E. M., 2015, *AJ*, 812, 90
- Navarro J. F., Frenk C. S., White S. D. M., 1997, *ApJ*, 490, 493
- Pakmor R., Pfrommer C., Simpson C. M., Springel V., 2016, *ApJ*, 824, L30
- Papadopoulos P. P., 2010, *AJ*, 720, 226
- Ruszkowski M., Yang H.-Y. K., Zweibel E., 2017, *ApJ*, 834, 208
- Salem M., Bryan G. L., 2014, *MNRAS*, 437, 3312
- Sarazin C. L., White R. E. I., 1987, *ApJS*, 320, 32
- Scoville N. Z., Yun M. S., Bryant P. M., 1997, *ApJ*, 484, 702
- Simpson C. M., Pakmor R., Marinacci F., Pfrommer C., Springel V., Glover S. C. O., Clark P. C., Smith R. J., 2016, *ApJ*, 827, L29
- Tomisaka K., Ikeuchi S., 1986, *PASJ*, 38, 697
- Toomre A., 1963, *ApJ*, 138, 385
- Uhlig M., Pfrommer C., Sharma M., Nath B. B., Enßlin E. A., Springel V., 2012, *MNRAS*, 423, 2374
- Vogelsberger M., Genel S., Sijacki D., Torrey P., Springel V., Hernquist L., 2013, *MNRAS*, 438, 1985
- Vogelsberger M., et al., 2014, *MNRAS*, 444, 1518
- Wiener J., Pfrommer C., Oh S. O., 2017, *MNRAS*, 467, 906
- Yabe T., Xiao F., 1993, *J. Phys. Soc. Japan*, 62, 2537
- ULIRG2016

This paper has been typeset from a $\text{\TeX}/\text{\LaTeX}$ file prepared by the author.